

Coupled pair of one and two dimensional magneto-plasmons on electrons on helium.

A.D. Chepelianskii,¹ D. Papoular,² H. Bouchiat,¹ and K. Kono³

¹*LPS, Univ. Paris-Sud, CNRS, UMR 8502, F-91405, Orsay, France*

²*LPTM, UMR 8089 CNRS & Univ. CergyPontoise, France*

³*ICST, NCTU, 1001 Ta Hsueh Rd., Hsinchu 300, Taiwan*

(Dated: October 18, 2019)

Electrons on the liquid helium surface form an extremely clean two dimensional system where different plasmon-excitations can coexist. Under a magnetic field time reversal symmetry is broken and all the bulk magneto-plasmons become gaped at frequencies below cyclotron resonance while chiral one dimensional edge magneto-plasmons appear at the system perimeter. We theoretically show that the presence of a homogeneous density gradient in the electron gas leads to the formation of a delocalized magneto-plasmon mode in the same frequency range as the lowest frequency edge-magnetoplasmon. We experimentally confirm its existence by measuring the corresponding resonance peak in frequency dependence of the admittance of the electron gas. This allows to realize a prototype system to investigate the coupling between a chiral one-dimensional mode and a single delocalized bulk mode. Such a model system can be important for the understanding of transport properties of topological materials where states of different dimensionality can coexist.

The recent discovery of topological states of matter has lead to striking predictions of topological surfaces and edge states [1–11]. However, it has so far been difficult to realise a system where topological edge states are completely decoupled from remaining bulk states or spurious edge states of non-topological origin [10–13]. Thus understanding the interaction between topological edge modes and non-topological bulk modes is highly important. Electrons on helium are a high purity two dimensional system where chiral edge magnetoplasmons modes naturally form under a perpendicular magnetic field [14–17], interestingly their topological origin has been recognized only recently [18–20]. Bulk magneto-plasmon in a two dimensional electron gas have a gap at frequencies below the cyclotron resonance, and it is traditionally considered that edge-magnetoplasmons are the only low frequency plasmon excitations [21, 22]. In experiments with electrons on helium the frequency of edge magnetoplasmons (EMP) is typically in the kHz range, while the cyclotron resonance frequency is typically several GHz. We show how a low energy bulk mode can be created inside the bulk-magnetoplasmon gap by an anisotropic gradient of electronic density. In this letter we will describe this plasma excitation as a magneto-gradient mode. We show that the frequency of this magneto-gradient mode can be obtained from an effective Schrödinger equation allowing to control the resonance frequency through the shape of the electron cloud. This allows to tune this frequency into resonance with the edge magnetoplasmons creating a model setting to study the interaction between bulk and topological edge modes. We note that the existence of this low frequency bulk magneto-plasmon can also be important to understand the surprising collective effects that appear in electrons on helium in the microwave induced resistance oscillation regime [23–29]: zero-resistance states [30, 31] and incompressibility [32, 33] which are not yet understood

microscopically.

We first show that the presence of a density gradient can indeed lead to the formation of a low frequency delocalized magneto-plasmon, this may seem counter-intuitive as in an homogeneous system all the bulk magneto-plasmons are gaped with their lowest frequency given by the cyclotron frequency $\omega_c = eB/m$. The equations of motion for magnetoplasmons can be derived from the drift diffusion equations on the electronic density $n_e = n_a + n_t$ where we decompose the electronic density into time averaged and time dependent parts. Treating the time-dependent terms as a small perturbation, we can linearise the drift diffusion equations which describe the electron flow on the liquid helium surface (see a sketch of the cell geometry in Fig. 1):

$$\partial_t n_t = \text{div}_{2d} [n_a (\mu_{xx} \nabla_{2d} V_t + \mu_{xy} \mathbf{u}_z \times \nabla_{2d} V_t)] \quad (1)$$

Here V_t is the time dependent part of the quasi-static electric potential $V = V_s + V_t$, in deriving this equation we took into account that the electron cloud screens the static-part of the electronic potential which leads to $\nabla V_s = 0$, the longitudinal and Hall mobilities are given by μ_{xx} and μ_{xy} . Experiments typically take place in the high magnetic field regime $\mu_{xx} \ll \mu_{xy}$ and $\mu_{xy} \simeq B^{-1}$ (this corresponds to ω_c much faster than the scattering rate). Hence it is reasonable to first find the frequency of the resonant plasmon modes in the limit $\mu_{xx} = 0$. The potential V_t can be determined from the time dependent density n_t by solving the electrostatic Poisson equation, for simplicity we will assume for now a local electrostatics approximation $n_t = \chi V_t$ where the compressibility $\chi = \frac{4\epsilon_0}{he}$ is obtained from a plane capacitor model. Simulations with an exact solution of electrostatic equations will be presented later. The static electron density in presence of a density gradient can be written as $n_a(r, \theta) = n_0(r) + n_{0c}(r) \cos \theta$ where (r, θ) are polar coordinates on the helium surface oriented along the gradient

direction. Away from the edges of the electron gas, we can approximate $n_{0c}(r) = \lambda r$ and treat the gradient λ as a small parameter anisotropy parameter. It is thus natural to expand n_t and V_t in harmonics of the angle θ :

$$n_t = n_{t0}(r) + n_{tc}(r) \cos \theta + n_{ts}(r) \sin \theta \quad (2)$$

where we have kept the lowest harmonics. This procedure is justified since the only anisotropy comes from the uniform density gradient which couples only nearby harmonics through the $\cos \theta$ term. Expanding the continuity equation to the lowest polar angle harmonics Eq. (1) we find an effective Schrödinger equation which describes standing-modes of electron-density oscillations:

$$\frac{\chi^2 \omega^2}{\mu_{xy}^2} \psi = -\frac{\lambda^2}{2} \partial_r^2 \psi + \frac{3\lambda^2}{8r^2} \psi + \frac{(\partial_r n_0)^2}{r^2} \psi \quad (3)$$

in this equation we introduced the effective wavefunction $\psi(r) = \sqrt{r} n_{ts}$ and ω is the frequency of the density oscillation, its time dependence obeys $\partial_t^2 \psi = -\omega^2 \psi$. This equation describes a radial wave which propagates at velocity $v = \mu_{xy} \lambda / \sqrt{2} \chi$. As in quantum mechanics, the shape of the wavefunction ψ is controlled by the external potential. From Eq. (3) we see that it contains a term describing repulsion at the origin and a confinement term proportional to the square of the gradient of the static isotropic density distribution $(\partial_r n_0)^2$. The obtained plasmon mode exists only due to the simultaneous presence of a magnetic field and of the anisotropic density gradient λ , we will thus call it a magneto-gradient plasmon (MGP). The frequency, ω_g , of first MGP mode is given by the ground state of the Schrödinger equation Eq. (3), it scales as $\omega_g \sim \mu_{xy} \lambda / (\chi R)$ where R is the radius of the electron cloud. This frequency vanishes the limit $R \rightarrow \infty$, its behaviour is thus similar to EMP which also do not have a gap and can have frequencies much below ω_c . The MGP frequency drops to zero at $\lambda = 0$ and will be overdamped if the density gradients are not strong enough. Fortunately due to the high mobilities of the electrons on helium system this mode can be visible even for small density gradients. Since Eq. (3) is a standing wave equation, in addition to the lowest frequency mode ω_g resonances are expected around its harmonics $\omega_n = n\omega_g$ ($n \geq 1$ an integer), these harmonics will however turn out to be overdamped in our experiments.

The previous calculation showed that a small density gradient can create delocalised bulk magneto-plasmon modes well below the cyclotron resonance frequency, which is usually believed to give the gap frequency for bulk magneto-plasmons. This calculation was performed using a local density approximation $n_t = \chi V_t$, and does not provide a complete description of the low frequency magneto-plasmon modes. Indeed Eq. (3) does not predict any finite frequency modes in the limit $\lambda \rightarrow 0$ and the edge magneto-plasmon modes are thus missing. Hence

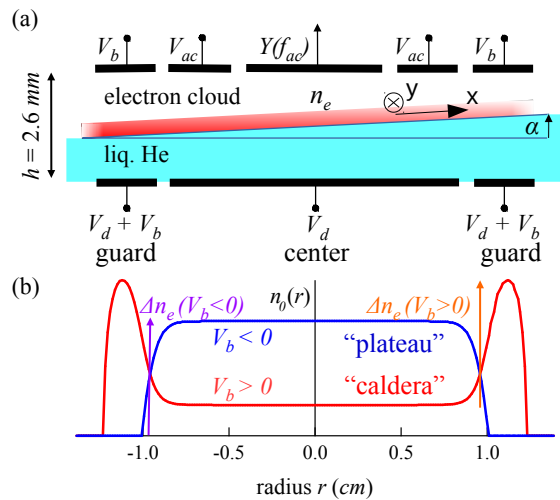


FIG. 1. (a) Sketch of the experimental cell with applied DC and AC voltages. The helium cell and electrodes have cylindrical symmetry but the helium level is slightly tilted with an angle α . A trapping potential $V_d = 7$ V is applied to all bottom electrodes and a bias voltage V_b can adjust the density between the outer guard and central regions. The cell admittance $Y(f_{ac})$ at frequency $f_{ac} = \omega/(2\pi)$ is measured between to central and middle electrodes on which an AC potential V_{ac} at frequency f_{ac} is applied. Panel (b) shows the typical “plateau” and “caldera” profiles which occur respectively at $V_b < 0$ and $V_b > 0$. Orange and purple arrows illustrate the two possible definitions of Δn_e in Eq. (4) for the two types of density profile.

a more realistic theory, reproducing the already known magnetoplasmons is thus needed. Such a theory has to go beyond the local density approximation and treat the long range Coulomb interactions in realistic way. This requires to fix the electrostatic environment of the electron gas and its properties. From here we will focus on a realistic model of our experimental setup with electrons on helium.

A sketch of the system is shown on Fig. 1, electrons are trapped on a helium surface by a pressing electric field. If the pressing electric field is perfectly perpendicular to the helium surface the geometry has cylindrical symmetry with respect to the polar angle θ and no gradient is present $\lambda = 0$. However a small misalignment angle α between the electric field direction and the normal of the helium surface leads to an in plane electric field component αE_{\perp} ($\alpha \ll 1$) which will create, within the local density approximation, a density gradient $\lambda = \chi \alpha E_{\perp}$. Since we assume that the helium surface remains flat in the region where electrons are confined, the drift diffusion equation Eq. (1) at the surface remain unchanged for finite α and it is only the relation between n_t and V_t which is changed when we use the exact non-local electrostatics. Since the normal of the electric field presents a discontinuity as it crosses the electrons on helium cloud, a direct perturbation theory expansion around the isotropic

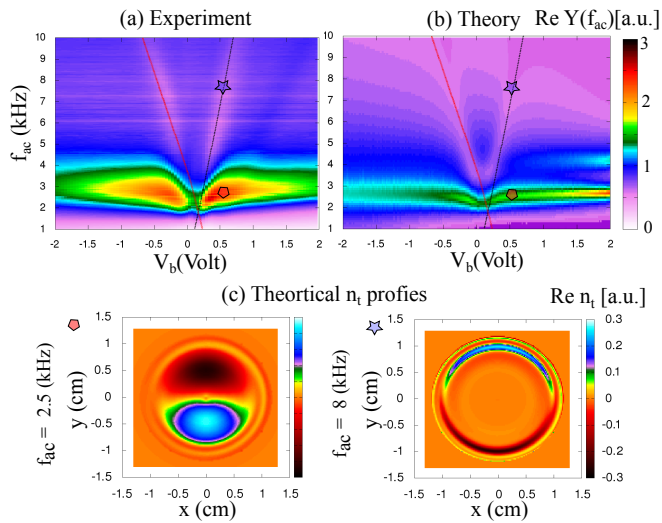


FIG. 2. (a) Magnetoplasmon modes appear as peaks in the real part of the cell admittance $Y(f_{ac})$ which is shown here as function of the density profile (controlled by the bias V_b between guard and central regions) and excitation frequency f_{ac} . Two magneto-plasmon modes are observed in the explored frequency range with very different dependence on V_b : a dispersing mode at higher frequency and a low frequency mode with very small dependence of the electron cloud density profile. (b) Finite element simulations of $Y(f_{ac})$ based on Eq. 1 taking into account a small tilt $\alpha = 0.4$ deg (fitted to data). (c) The simulations allow to represent the oscillating density profile n_t , the low frequency “magneto-gradient” plasmon (polygon symbol) is delocalised across all the electron cloud, whereas the higher frequency plasmon (star symbol) is an edge magneto-plasmon (or inter-edge at $V_b > 0$) propagating in one-dimension, the two modes seem to make an avoided crossing when their frequencies overlap near $V_b = 0$.

solution is not possible. We derived a suitable perturbation theory expansion by performing a transformation into a curved set of coordinates where the position of the interface remains fixed with α . This expansion, to the lowest order, leads to a modified Laplace equation which is given in Appendix. Finite elements (FEM) [34] simulations based on this equation, confirm the validity of the approximation $n_{0c}(r) \simeq \alpha \chi E_{\perp} r$ for all the shapes of the electron cloud explored experimentally except near the edge of the electron cloud. Thus a small inclination of the helium surface with respect to the helium cell creates a well defined density gradient which only weakly depends on the shape of the electron cloud $n_0(r)$. To simulate approximately the AC response of electrons on helium, we used the Poisson equation on AC potential in the limit $\alpha = 0$ and drift diffusion equations on the helium surface to determine the expected admittance of the cell. The full equations and a discussion on their formal validity are provided in Appendix.

We now present experiments that reveal the co-existence of 1D EMP and 2D MGP plasmons, the simulations, which are presented simultaneously, will al-

low to confirm the identification of the observed modes. The experiments were realised on an electron cloud (see Fig. 1) with $N_e = 3 \times 10^7$ electrons at a magnetic field of $B_z = 0.3$ Tesla and temperature of 300mK. The AC transport response of the electron cloud is measured in a Corbino geometry using a Sommer-Tanner method. An AC excitation voltage V_{ac} with a 30mV amplitude is applied on the intermediate top-ring electrode at a frequency f_{ac} (1 to 10 kHz) and the induced pick-up signal from the top central electrode is then measured with a voltage amplifier and a lock-in detector giving the AC cell admittance $Y(f_{ac})$. The position of magneto-plasmon resonances then shows as peaks in the admittance $Y(f_{ac})$ for a fixed bias voltage V_b . This bias between the outer guard and central electrodes can tune the frequency of the magneto-plasmons by controlling the shape of the electron cloud [32, 35]. For $V_b < 0$ the electron cloud adopts a “plateau” density profile, where the density $n_0(r)$ is a monotonously decaying function of the radial distance to the cloud center r , while for $V_b > 0$ the electron density takes a “caldera” profile which has a density maximum inside the guard region at edge of the electron cloud (Fig. 1b). The EMP which couple to the top measuring electrodes are different in the two regimes. For a “plateau” profile the outer-edge of the cloud is closer to the center and it is the EMP propagating at the perimeter of the cloud which are detected. For a “caldera” profile the cloud expands and the outer-perimeter becomes weakly coupled to the measurement electrodes, instead it is the inter-edge magneto-plasmon at the boundary between the guard and central regions which is more easily excited. To simplify further discussions we will describe both situations as an EMP mode. The theoretical expressions for the propagation velocity are indeed similar in both cases [17, 21]:

$$v_{EMP} \simeq \frac{\Delta n_e}{2\pi\epsilon_0 B} \ln \frac{1}{qh} \quad (4)$$

where q is the wave vector ($q = 1/R$ for the lowest frequency mode where R is the radius of central bottom electrode) and Δn_e the difference in electron density between the electron density in the center and guard regions (this definition is discussed in more precisely below).

For the magneto-gradient plasmon the propagation velocity is given by:

$$v_{MGP} \simeq \frac{\alpha E_{\perp}}{B\sqrt{2}} \quad (5)$$

this expression is obtained from Eq. (3) using the approximation $\lambda = \alpha \chi E_{\perp}$. It depends on the perpendicular electric field E_{\perp} but not on Δn_e as opposed to the EMP modes. This difference in the Δn_e dependence provides a convenient method to distinguish between MGP and EMP modes. We represent the admittance $Y(f_{ac})$ as function of both V_b and f_{ac} as a color scale map that

allows to visualize the dependence of the mode frequency on the voltage V_b (and thus on Δn_e). Modes that “disperse” as function of V_b are candidate 1D EMP modes while the absence of a V_b dependence suggests a magneto-gradient mode.

Our experimental results are shown on Fig. 2 together with FEM simulations of the perturbation theory that we introduced. Both experiment and simulations show the presence of two resonant modes at low frequency. A mode whose frequency that strongly depends on V_b with a dependence that reminds the dispersion relation of “Dirac” fermions, and a second mode whose frequency is almost independent on V_b except when its frequency crosses the frequency of the dispersive mode.

To identify the dispersive mode as an EMP we show the theoretical frequency expected from Eq. (4). For the “calderia” geometry (positive V_b , black lines), we set Δn_e as the difference between the electron density on top of the rim in the guard region and the density in the center of the electron-cloud, it reproduces the experimental EMP frequency without adjustable parameters. For the plateau geometry (red line for negative V_b) the density in the guard entering in Δn_e had to be reduced by 20% compared to its maximum density in the guard. This phenomenological correction probably reflects a more complex situation where the boundary of the electron cloud boundary moves with V_b as the cloud is pushed towards the center. FEM simulations predict the correct position for the EMP mode without adjustable parameters even in this case. The predictions for the linewidth and admittance amplitude are less accurate as they dependent on the ratio μ_{xx}/μ_{xy} which was assumed to be fixed to 5×10^{-3} and without any density dependence. To confirm the 1D character of this dispersive mode we also represented the simulated oscillating density profile n_t of the EMP mode on Fig. 2, the oscillating density is indeed localised in a narrow strip of width h at the boundary between the central and guard regions. Note that, the perturbation theory is not reliable at the outer edge of the electron cloud and the peak in n_t on the outer cloud boundary may not be physical.

The lowest frequency mode on Fig. 2 has a resonance frequency which is independent of V_b except near the crossing points with the previously identified EMP mode. It is thus a candidate magneto-gradient plasmon (MGP) mode. To confirm this assignment, we checked that this frequency scales as $\propto E_{\perp}/B$ as expected from Eq. (5). The only other parameter in Eq. (5) is the inclination of the helium free surface α compared to the electric field. It was not possible to control this angle precisely in our experiment however we confirmed that this frequency changes indeed with a small variation (of around 0.1 deg) of the fridge inclination (all other parameters were kept fixed). The FEM simulations confirm the existence of the low frequency magneto-gradient mode. As can be seen from its oscillating density profile on Fig. 2,

this mode is indeed delocalised across the entire electron cloud. The FEM simulations can be used to fix the tilt angle α , in Fig. 2 a good agreement far from the crossing with the EMP mode is obtained for $\alpha = 0.4\text{deg}$. At the crossing both simulations and experiment suggest an avoided crossing between the MGP and EMP modes which implies the exciting possibility of realizing hybrid states with simultaneous characteristics of a one dimensional topological EMP and a delocalised two dimensional mode. Investigation such hybrid states requires more detailed experimental and theoretical investigations. Concerning the linewidth of MGP modes the simulations predict a similar linewidth to the edge magnetoplasmon modes. This contrasts with the experiment where the MGP is significantly broader than the EMP with a linewidth that depends on V_g . This could be due to the dependence of the mobility on the electron density which is not taken into account in the model. Indeed MGP is delocalized and thus can be more sensible to mobility gradients which appear as a result of the density variations across the electron cloud. In the simulations we fixed the ratio μ_{xx}/μ_{xy} to reproduce the linewidth of the EMP mode, the linewidth of the MGP is thus underestimated compared to the experiment. The simulations thus resolve the next MGP harmonic at positive V_b which not visible experimentally as it is probably overdamped.

To sum up, we have shown both theoretically and experimentally that a system of electrons on the surface of liquid helium hosts a novel type of bulk excitation, the delocalized two-dimensional magnetogradient plasmon modes which appear in the presence of a small density gradient. This system provides a highly controllable environment in which the interaction of this novel excitation with the previously known (topological) one-dimensional edge magnetoplasmons may be studied. As gradients of carrier concentration can easily be present in mesoscopic devices, this mode can also exist in new two dimensional electrons systems with high mobility.

We acknowledge fruitful discussions with D. Konstantinov, D.L. Shepelyansky and M. Dykman and thank ANR SPINEX for financial support.

-
- [1] C. L. Kane and E. J. Mele, Physical Review Letters **95**, 1 (2005), arXiv:0411737v2 [cond-mat].
 - [2] B. Bernevig, T. Hughes, and S. Zhang, Science (New York, N.Y.) **314**, 1757 (2006), arXiv:0611399 [cond-mat].
 - [3] M. König, S. Wiedmann, C. Brüne, A. Roth, H. Buhmann, L. W. Molenkamp, X.-L. Qi, and S.-C. Zhang, Science (New York, N.Y.) **318**, 766 (2007), arXiv:0710.0582.
 - [4] L. Fu and C. L. Kane, Phys. Rev. B **76**, 045302 (2007).
 - [5] S. Murakami, New Journal of Physics **9** (2007), 10.1088/1367-2630/9/9/356, arXiv:0710.0930.
 - [6] D. Hsieh, D. Qian, L. Wray, Y. Xia, Y. S. Hor, R. J. Cava, and M. Z. Hasan, Nature **452**, 970 (2008), arXiv:0910.2420.

- [7] Y. L. Chen, J. G. Analytis, J.-H. Chu, Z. K. Liu, S.-K. Mo, X. L. Qi, H. J. Zhang, D. H. Lu, X. Dai, Z. Fang, S. C. Zhang, I. R. Fisher, Z. Hussain, and Z.-X. Shen, *Science* **325**, 178 (2009).
- [8] A. A. Taskin, Z. Ren, S. Sasaki, K. Segawa, and Y. Ando, *Phys. Rev. Lett.* **107**, 016801 (2011).
- [9] I. Knez, R.-R. Du, and G. Sullivan, *Phys. Rev. Lett.* **107**, 136603 (2011).
- [10] A. Murani, A. Kasumov, S. Sengupta, Y. A. Kasumov, V. T. Volkov, I. I. Khodos, F. Brisset, R. Delagrè, A. Chepelianskii, R. Deblock, H. Bouchiat, and S. Guéron, *Nature Communications* **8**, 15941 EP (2017), article.
- [11] F. Schindler, Z. Wang, M. G. Vergniory, A. M. Cook, A. Murani, S. Sengupta, A. Y. Kasumov, R. Deblock, S. Jeon, I. Drozdov, H. Bouchiat, S. Guéron, A. Yazdani, B. A. Bernevig, and T. Neupert, *Nature Physics* **14**, 918 (2018).
- [12] E. B. Olshanetsky, Z. D. Kvon, G. M. Gusev, A. D. Levin, O. E. Raichev, N. N. Mikhailov, and S. A. Dvoretzky, *Phys. Rev. Lett.* **114**, 126802 (2015).
- [13] S. Mueller, A. N. Pal, M. Karalic, T. Tschirky, C. Charpentier, W. Wegscheider, K. Ensslin, and T. Ihn, *Phys. Rev. B* **92**, 081303 (2015).
- [14] D. C. Glatli, E. Y. Andrei, G. Deville, J. Poitrenaud, and F. I. B. Williams, *Phys. Rev. Lett.* **54**, 1710 (1985).
- [15] D. B. Mast, A. J. Dahm, and A. L. Fetter, *Phys. Rev. Lett.* **54**, 1706 (1985).
- [16] I. Petković, F. I. B. Williams, K. Bennaceur, F. Portier, P. Roche, and D. C. Glatli, *Phys. Rev. Lett.* **110**, 016801 (2013).
- [17] V. A. Volkov and S. A. Mikhailov, *Zh. Eksp. Teor. Fiz.* **94**, 217 (1988).
- [18] D. Jin, L. Lu, Z. Wang, C. Fang, J. D. Joannopoulos, M. Soljacic, L. Fu, and N. X. Fang, *Nature Communications* **7**, 13486 EP (2016).
- [19] D. Jin, Y. Xia, T. Christensen, S. Wang, K. Y. Fong, M. Freeman, G. C. Gardner, S. Fallahi, Q. Hu, Y. Wang, L. Engel, M. J. Manfra, N. X. Fang, and X. Zhang, arXiv:1803.02913.
- [20] T. Ozawa, H. M. Price, A. Amo, N. Goldman, M. Hafezi, L. Lu, M. C. Rechtsman, D. Schuster, J. Simon, O. Zeitlinger, and I. Carusotto, *Rev. Mod. Phys.* **91**, 015006 (2019).
- [21] V. A. Volkov and S. A. Mikhailov, *Modern Problems in Condensed Matter Sciences* **27**, 855 (1991).
- [22] I. L. Aleiner, D. Yue, and L. I. Glazman, *Phys. Rev. B* **51**, 13467 (1995).
- [23] M. A. Zudov, R. R. Du, J. A. Simmons, and J. L. Reno, *Phys. Rev. B* **64**, 201311 (2001).
- [24] P. Ye and L. Engel, *Appl. Phys. Lett.* **79**, 2193 (2001).
- [25] R. Mani, S. J.H., K. K., N. V., W. B.J., and U. V., *Nature* **420**, 646 (2002).
- [26] M. Zudov, R. Du, L. Pfeiffer, and K. West, *Phys. Rev. Lett.* **90**, 045807 (2003).
- [27] R. G. Mani, A. N. Ramanayaka, and W. Wegscheider, *Phys. Rev. B* **085308**, 085308 (2011).
- [28] Y. P. Monarkhaa, *Low Temp. Phys.* **37**, 655 (2011).
- [29] I. A. Dmitriev, A. D. Mirlin, D. G. Polyakov, and M. A. Zudov, *Rev. Mod. Phys.* **84**, 1709 (2012).
- [30] D. Konstantinov and K. Kono, *Phys. Rev. Lett.* **103**, 266808 (2009).
- [31] D. Konstantinov and K. Kono, *Phys. Rev. Lett.* **105**, 226801 (2010).
- [32] A. D. Chepelianskii, M. Watanabe, K. Nasyedkin, K. Kono, and D. Konstantinov, *Nature Communications* **6**, 7210 EP (2015), article.
- [33] D. Konstantinov, A. Chepelianskii, and K. Kono, *Journal of the Physical Society of Japan* **81**, 093601 (2012), <https://doi.org/10.1143/JPSJ.81.093601>.
- [34] F. Hecht, *J. Numer. Math.* **20**, 251 (2012).
- [35] A. Chepelianskii, M. Watanabe, and K. Kono, *J. Low Temp. Phys.* **195**, 307 (2019).

APPENDIX

Derivation of the effective Schrödinger equation Eq. (3) This equation is derived from the drift diffusion equations written in the local density approximation:

$$\partial_t \begin{cases} n_{t0} \\ n_{tc} \\ n_{ts} \end{cases} = \frac{\mu_{xy}}{\chi r} \begin{cases} \lambda \partial_r (r n_{ts}) / 2 \\ n_{ts} \partial_r n_0 \\ \lambda r \partial_r n_{t0} - n_{tc} \partial_r n_0 \end{cases} \quad (6)$$

The density gradient λ introduces a coupling between different angular harmonics of the electron density, introducing the effective wavefunction $\psi(r) = \sqrt{r} n_{ts}$ this equation can be reduced to the effective Schrödinger equation Eq. (3).

Effective Poisson equation in deformed coordinates where the position of the helium layer is fixed.

To enable the use of standard perturbation series we thus need to perform a coordinate transformation which levels the helium surface in the cell while keeping in place the top and bottom electrodes. We choose a rotation in the (x, z) plane (containing the electric field direction z and the slightly miss-aligned helium surface normal) with a height dependent rotation angle $\phi(z) = \alpha \left(1 - \frac{4z'^2}{h^2}\right)$. The transformation between coordinates is realized by:

$$\begin{pmatrix} x \\ z \end{pmatrix} = \begin{pmatrix} \cos \phi(z') x' - \sin \phi(z') z' \\ \sin \phi(z') x' + \cos \phi(z') z' \end{pmatrix} \quad (7)$$

where x', z' are the new coordinates.

In the new coordinates the Poisson equation, to first order in α , becomes:

$$\Delta V + \frac{8\alpha}{h^2} (x \partial_z V + 2xz \partial_z^2 V - 3z \partial_x V - 2z^2 \partial_{xz} V) = 0 \quad (8)$$

in this form it can be expanded in powers of α . We see from Eq. (8) that α induces a coupling only between neighboring angular harmonics, thus to first order in α to which we will limit ourselves here, only $\cos \theta$ and $\sin \theta$ terms will be generated.

We solved Eq. (8) for a stationary electron cloud without AC excitation, this allows us to find the static density profile $n_a(r, \theta) = n_0(r) + \alpha n_{0c}(r) \cos \theta$ induced by the tilt of the cell. In the stationary case the potential of the electron cloud is constant and fixed by the total charge of the cloud. In the isotropic case the problem then reduces to find a stable boundary of the electron cloud for which the electric field at the boundary vanishes, which was done in a systematic way for different geometries in [32]. To find the anisotropic correction $n_{0c}(r)$ we iterated Eq. (8) neglecting the small deformation of the circular cloud boundary. While this approach should give accurate predictions in the center of the electron cloud, the validity of the perturbation theory breaks down near the cloud boundary. The results of our finite element calculations for $n_0(r)$ and $n_{0c}(r)$ are shown below on Fig.3.

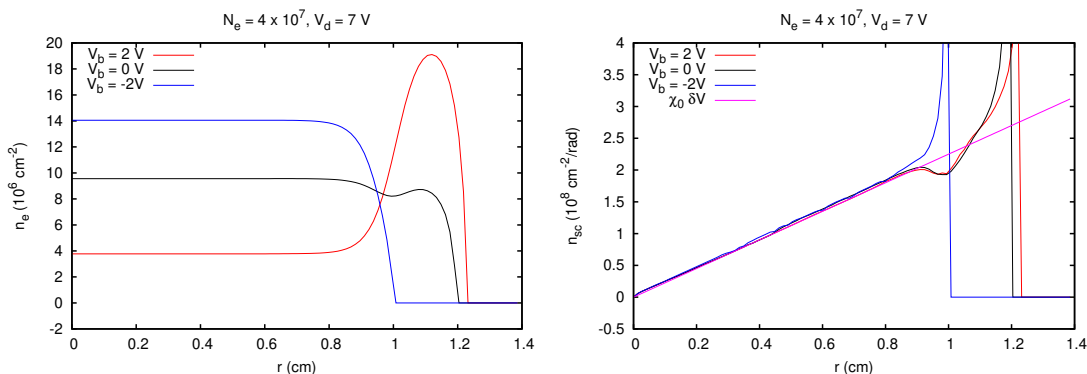


FIG. 3. Left hand side panel shows the evolution of the radial steady state density $n_0(r)$ for different bias voltages V_b between central and guard reservoirs. The right hand side panel shows the tilted component of density n_{0c} under the same conditions (we remind that the total steady state density is the sum $n_0(r) + \alpha n_{0c}(r) \cos \theta$), n_{0c} depends only weakly on V_b in contrast to $n_0(r)$ and is well approximated by $n_{0c} = \chi \alpha E_{\perp} r$ (straight line).

To be fully consistent we in principle need to use the modified Poisson equation Eq. (8) which introduces a mixing between harmonics due to the tilt, we found however that using the usual Poisson equation $\Delta V = 0$ gives already

a good description of the experiment. This probably comes from the fact that the dynamic drift-diffusion equations already introduces a coupling between modes through the density gradient n_{0c} and many (but seemingly not all) of the terms that would come from Eq. (8) become second order in α .

Full drift diffusion equations for the lowest angular harmonics For reference we write the full drift diffusion equations as a function of the steady state radial distribution n_0 and the density gradient n_{0c} including contributions from both μ_{xx} and μ_{xy} , these are the equations which are solved to build Fig. 2 in the main text.

The AC potential V_t is decomposed into its lowest harmonics $V_t = V_{t0}(r) + V_{tc}(r) \cos \theta + V_{ts}(r) \sin \theta$.

$$\partial_t \begin{pmatrix} n_{t0} \\ n_{tc} \\ n_{ts} \end{pmatrix} = \frac{\mu_{xy}}{r} \begin{pmatrix} \frac{1}{2} \partial_r (n_{sc} V_{ts}) \\ V_{ts} \partial_r n_0 \\ n_{sc} \partial_r V_{t0} - V_{tc} \partial_r n_0 \end{pmatrix} + \frac{\mu_{xx}}{r} \begin{pmatrix} \partial_r [r(n_0 \partial_r V_{t0} + \frac{1}{2} n_{sc} \partial_r V_{tc})] \\ \partial_r [r(n_0 \partial_r V_{tc} + n_{sc} \partial_r V_{t0})] - \frac{n_0}{r} V_{tc} \\ \partial_r [r(n_0 \partial_r V_{ts})] - \frac{n_0}{r} V_{ts} \end{pmatrix} \quad (9)$$